Computers and Geotechnics 167 (2024) 106089

Contents lists available at ScienceDirect

Computers and Geotechnics

journal homepage: www.elsevier.com/locate/compgeo

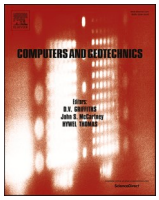

Research Paper

Considerations for using critical state soil mechanics based constitutive models for capturing static liquefaction failure of tailings dams

Haoyuan Liu [a,*], Sparsha Nagula [b], Hans Petter Jostad [b,*], Luca Piciullo [b], Farrokh Nadim [b]

[a] Beihang University, Beijing, China
[b] Norwegian Geotechnical Institute, Oslo, Norway

ARTICLE INFO

Keywords:
Tailings dam
Static liquefaction
Constitutive model
FEM
Stability

ABSTRACT

Recent disastrous tailings dam failures have heightened public concerns about the safety of these structures. Typically, tailings are disposed of as a slurry in a loosely saturated state, making them susceptible to static liquefaction. The widely used limit equilibrium method for analysing tailings dams may overlook potential failures and is incapable of simulating static-liquefaction-type dam failures. This paper presents simulations of the initiation of progressive failure within a finite element framework, using a well-described tailings dam in Brazil as a basis. Three different constitutive models (Hardening Soil, SANISAND2004, and NorSand) were employed to demonstrate a numerical modelling procedure for simulating tailings dam static liquefaction and a practical approach to numerically account for the effects of fines content in slime layers. Models that incorporate the state parameter (ψ) as an integral part can realistically depict the loss of strength in loose granular materials during a liquefaction process. Stress–strain paths of representative points in critical zones of the studied tailings dam indicate localized shear deformations that lead to progressive failure due to static liquefaction.

1. Introduction

Tailings are a mixture of sand, silt, and clay with a high content of unrecoverable metals, chemical reagents, and process water used during the extraction of raw materials. Typically, tailings are discharged into a final storage area known as a Tailings Storage Facility (TSF), often retained by dams or embankments. The uncertainties in the physical and chemical characteristics of tailings have led to several catastrophic tailings dam failures. Upstream-constructed tailings dams are more prone to failure than downstream dams (Wei et al., 2013; Piciullo et al., 2022). The failure of a tailings dam can result in the release of slurry that can travel over hundreds of kilometers, causing fatalities, polluting the environment, and damaging local ecosystems and communities (Glotov et al., 2018; Yu et al., 2020; Rotta et al., 2020).

Among various failure mechanisms, the static liquefaction mode of failure in saturated tailings dams is common (Sadrekarimi, 2016; Gens, 2019) and is the least understood. The tailings deposited hydraulically are possibly in a loose state due to the lack of compaction after deposition. Abrupt liquefaction is likely to occur in loose saturated material with a certain amount of disturbance (Gens, 2019). This abrupt liquefaction corresponds to 'spontaneous liquefaction' (Terzaghi, 1957) and may be explained by the concept of negative second-order work (Nicot et al., 2011). The various forms of disturbances that can initiate liquefaction can be classified as follows (Martin and McRoberts, 1999; Gens, 2019): (1) construction (and possibly other activities) induced load increase on the dam surface, (2) lateral stress reduction, (3) changes in pore water pressures, and (4) vibrational loads. Despite the different triggering approaches, it should be noted that static liquefaction is recognized as a type of undrained behavior that can occur in loose granular materials triggered by a monotonically increasing shear load (Sadrekarimi, 2014).

Simulating the failure of a tailings dam induced by construction activity in a static-liquefaction manner is challenging. When it comes to the stability analysis of loose, saturated, and brittle soils, the use of limit equilibrium methods can lead to an oversight of potential tailings dam failures. Therefore, various researchers have employed finite element and finite difference methods to gain a better understanding of tailings dam slopes and tailings ponds (Brzezinski, 2002; Zandarín et al., 2009; Guo et al., 2020; Tang et al., 2022; Peter and Mahmood, 2003; Wang et al., 2011; Chakrabotry and Choudhury, 2009). The construction phase in the time domain involves the gradual increase of the dam height and the spontaneous generation/dissipation of pore water. A catastrophic

* Corresponding authors at: Beihang University, Beijing, China (H. Liu); Norwegian Geotechnical Institute, Oslo, Norway (H. Petter Jostad).
E-mail addresses: liuhy6955@163.com, haoyuan.liu@ngi.no (H. Liu), hans.petter.jostad@ngi.no (H. Petter Jostad).

https://doi.org/10.1016/j.compgeo.2024.106089
Received 21 August 2023; Received in revised form 10 December 2023; Accepted 8 January 2024
Available online 19 January 2024

tailings dam failure of the static-liquefaction type can occur due to a small perturbation under undrained conditions. Capturing such an instance is difficult as it is related to the stress field, drainage conditions, and the magnitude of the perturbation. Another challenge in realistically simulating tailings dams, although not directly linked to static liquefaction, is modeling the slime layers commonly found in tailings dams.

This study showcases the capability of a finite element framework to capture the phenomenon of static-liquefaction-induced collapse through the use of an appropriate constitutive model. The critical state theory (Roscoe et al., 1958; Schofield and Wroth, 1968; Jefferies and Been, 2006; among others) has proven indispensable in comprehending the abrupt transition from drained and seemingly stable conditions to an undrained liquefaction-driven collapse. Three distinct constitutive models—Hardening Soil (Schanz et al., 1999), SANISAND2004 (Dafalias and Manzari, 2004), and NorSand (Jefferies, 1993; Jefferies and Shuttle, 2005)—were employed to simulate the initiation of progressive failure within a finite element framework. This work introduces a numerical modelling procedure to simulate static liquefaction in tailings dams. It also provides a practical approach to incorporate the effects of fines content in slime layers by adjusting the critical state line based on the fines content. It is demonstrated that models incorporating the critical state theory with the state parameter (ψ) as an integral part can realistically depict the loss of strength in loose granular materials under undrained shearing. Stress–strain paths of representative points in critical zones indicate localized shear deformations that lead to progressive failure due to static liquefaction.

2. Scope and objectives

The objective of this study is to establish a numerical simulation methodology for modeling static liquefaction-induced failures in tailings dams, taking into account the influence of slime layers within the dam. In this study, the dam is assumed to be constructed under drained condition while the dam instability is triggered by increasing the self-weight of the material under undrained conditions. Such a triggering method corresponds to the increase of load as summarized by Martin and McRoberts (1999) and Gens (2019). The increase in self-weight is applied using the arch-length based load control available in PLAXIS (Brinkgreve et al., 2016). This enables the simulation of the entire failure process starting from the first instability point to the entire collapse of the dam (Section 5).

Critical soil mechanics based constitutive model having state parameter as state variable such as, SANISAND2004 (Dafalias and Manzari, 2004) and NorSand (Jefferies, 1993; Jefferies and Shuttle, 2005), are used in this work. Slime layers are modelled by varying their critical-state and strength-related model parameters based on the amount of fines in slime materials (Section 4 and Section 5.3). The initial stress fields generated by using the SANISAND2004 and NorSand model are compared with that of von Mises failure based Hardening soil (HS) model (Schanz et al., 1999) to understand the influence of initial stress state on dam stability (Section 6).

3. Description of the case study

This work utilized a tailings dam in Brazil as a case study to present the numerical simulation approach of static liquefaction-induced dam failure. The geometry and relevant dam material properties are well-documented and publicly available (Morgenstern et al., 2016). The section provides a detailed description of the geometry of the tailings dam that was modelled in the FE framework, along with the properties of the various tailings layers.

3.1. Dam geometry and tailings

The failure of the simulated tailings dam occurred abruptly while it was still in operation, with no prior warning. These raised suspicions of static liquefaction. Such 'abrupt undrained' failure can be caused by a small disturbance in a localized unstable zone of the tailings dam. The failure then propagated from these localized zones leading to a global dam collapse. The adopted cross-section of the dam is illustrated in Fig. 1. The dam was 700 m in length, and 92 m in height. Soil layers below the phreatic line were fully saturated prior to dam failure. The phreatic line was illustrated as the *AB* line in Fig. 1. The dam geometry and stratigraphy were obtained by post-processing and idealizing data from the GIS survey. The layers in the dam were categorized into bedrock, slimes, tailings sand (or sand), and compacted tailings (sand). The slimes were further subdivided according to the relative proportion of sand and slimes:

(1) predominantly slimes: 100 % slime properties.
(2) mixed sand and slimes: 50 % sand and 50 % slime properties.
(3) interbedded slimes: 80 % sand and 20 % slime properties.
(4) isolated slimes: 100 % sand properties, hence, isolated slimes were treated as sand tailings.

The presence of a weak layer was identified based on CPTu profiling, as indicated in Fig. 1. The weak layer was composed of sand tailings but with lower initial relative density.

3.2. Sand tailings and slimes

Morgenstern (2016) found that the sand tailings had an effective friction angle of $\phi' = 31.4^{\circ}$ as determined from direct simple shear tests, which was comparable to the effective friction angle of $\phi' = 32.8^{\circ}$ as determined from triaxial tests. The bulk unit weight of the sand tailings is $22\,\mathrm{kN/m^3}$. The coefficient of uniformity $C_u = 3.83$ and the coefficient of curvature $C_c = 1.39$. The grain size distribution curve of the sand is illustrated in Fig. 2. Approximately 40 ~ 45 % percent of the sand tailings grains were smaller than 0.075 mm. The permeability of sand tailings was found to be 3×10^{-6} m/s. The characteristics of slimes were found to be more similar to that of cohesive material than sand tailings. The slimes (predominantly slimes, mixed tailings and slimes, interbedded slimes) had a dry unit weight of $\gamma_d = 16.45\mathrm{kN/m^3}$ with a void ratio of 1.268 and specific gravity $G_s = 3.806$. The plasticity index of the slimes was 7 ~ 11. For the ease of comparison, uniform bulk unit weight of $22\,\mathrm{kN/m^3}$ was adopted. The slimes contained grains less than 0.075 mm in size (i.e., can be treated as fines), as indicated in Fig. 2. The slimes' permeability was found to be less than 1×10^{-8} m/s. The small strain shear modulus G_{max} was determined as per Equation (1), with equation coefficients given in Table 1 for different layers.

$$G_{max} = C_G \left(\frac{\sigma_v'}{p_{atm}} \right)^{R_G} \tag{1}$$

where, C_G is a constant, R_G defines stress-dependency, p_{atm} is the atmospheric pressure used for normalization, σ_v' is the vertical effective stress. G_{max} was found to decrease with increasing slime content at same stress level.

Both SANISAND2004 and NorSand models are based on the critical state soil mechanics theory. The input parameters of these models include the critical state line (CSL) parameters. CSL can be described using Equation (2) and (3).

$$e_c = \Gamma - \lambda ln(p') \tag{2}$$

$$e_c = e_{c0} - \lambda \left(\frac{p'}{p_{atm}} \right)^{\xi} \tag{3}$$

where, λ defines the slope of the CSL in the e_c logp' space, e_{c0} is the reference void ratio at $p' = 0kPa$, Γ represents the critical void ratio at $p' = 1kPa$, exponent ξ controls the curvature of CSL, p' is the mean

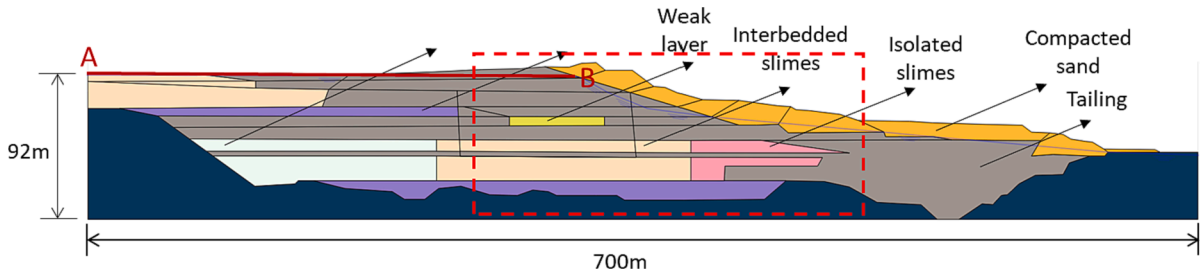

Fig. 1. Dam geometry and material distribution of the case study.

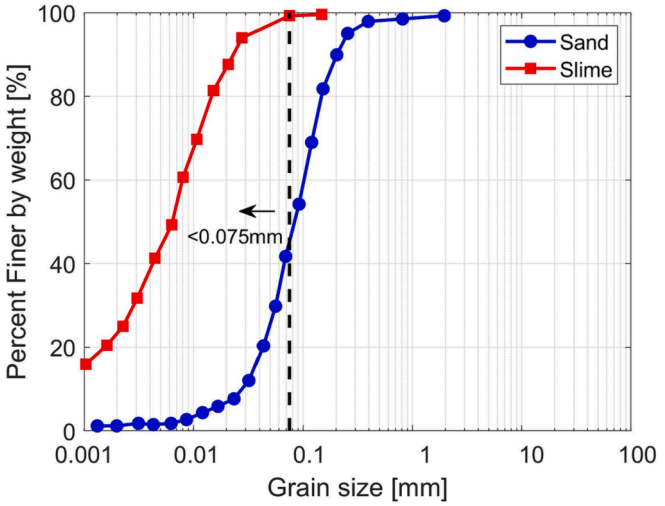

Fig. 2. Grain size distribution curves of sand and slimes.

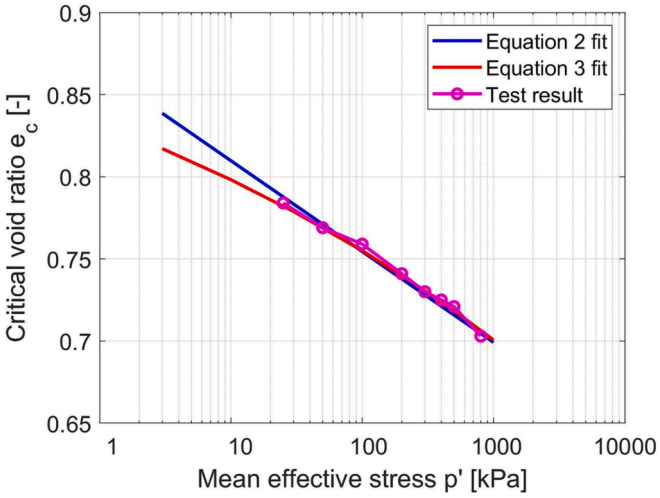

Fig. 3. Calibration of the critical state line for two different equations.

Table 1
Equation constants to determine the small strain shear modulus of different materials.

Material	C_G [MPa]	R_G [-]	Stiffness ratio*
Sand tailings and isolated slimes	60	0.4	1
Interbedded slimes	50.1	0.42	0.83
Mixed sand and slimes	35.1	0.47	0.58
Predominantly slimes	10.8	0.7	/**

* Estimated as the ratio between material G_{max} and the G_{max} of the sand tailings.

** Not easy to estimate due to the big different on the R_G values compare to other materials.

effective stress. Morgenstern et al. (2016) described the critical state line for sand tailings based on undrained and drained triaxial test results, as shown in Fig. 3.

The experimental data can be curve fitted using Equation (2) and (3) depending on different CSL shape assumptions in the e_c logp' space (Schofield and Wroth, 1968; Li and Dafalias, 2000).

Soil grains smaller than 0.075 mm are considered as fines hence, pure slimes are considered to have 100 % fines, and sand tailings have 40 % fines, as indicated in Fig. 2. Similarly, the fines content of each tailings dam layer was determined based on the percentage of sand tailings and slimes present in each layer. It was identified that sand tailings and isolated slimes had 40 % fines, interbedded slimes had 50 % fines, mixed sand and slimes had 70 % fines, and predominantly slimes had 100 % fines. Fines content has a significant impact on the mechanical behaviour of sand-silt mixtures. Yin et al. (2016) demonstrated that the location of the CSL changes with varying fines content in the sand-silt mixtures. Experimental evidence was provided based on the

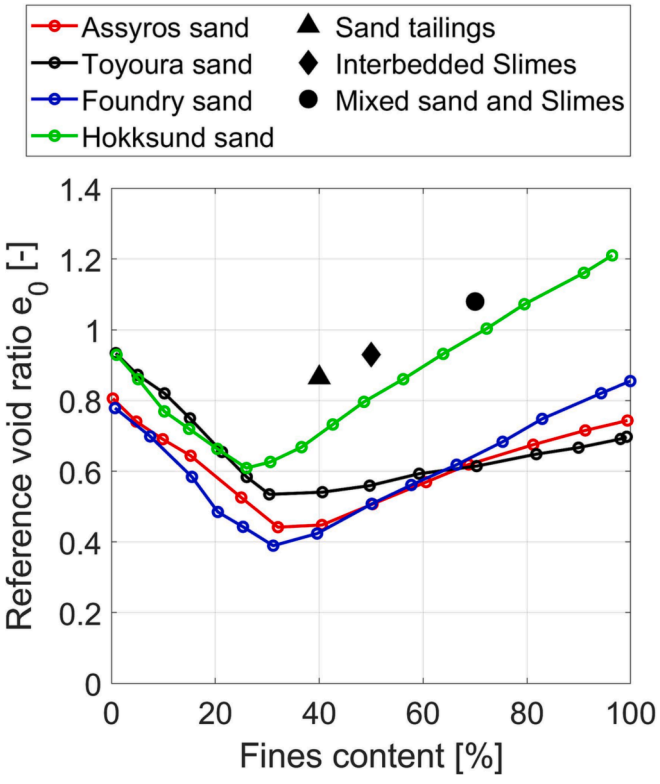

Fig. 4. Fines content effects on the reference critical void ratio e_{c0} (plot modified after Yin et al., 2016).

results from four types of sand, as shown in Fig. 4. Equation (3) was adopted to study the effects of fines content on the CSL location for the different tailings dam layers. The reference critical void ratio e_{c0} first decreased and then increased with increasing fines content, as illustrated in Fig. 4. The minimum e_{c0} occured around a fines content of 25 ~ 30 %.

The CSL line was assumed to vary as shown in Fig. 4 for the different layers of the tailings dam. The CSL retained the same shape for various fines content but considered different e_{c0} values, as illustrated in Fig. 4. The fines content in the various tailings dam layers in this study was found to be larger than 35 %, as discussed earlier. Beyond 30 % fines, the e_{c0} increases with increasing fines content, as indicated by the solid lines in Fig. 4. Assume that the change in the reference critical void ratio for sand tailings, interbedded slimes, and mixed sand and slimes follows the same trend as observed in Hokksund and Foundry sand from the literature (Fig. 4*)*. The reference critical void ratios for interbedded slimes and mixed sand and slimes are summarized in Table 2 and illustrated in Fig. 4.

4. Computational framework and constitutive model

4.1. PLAXIS 2D numerical model and analysis phases

A 2D plane strain model was created in PLAXIS 2D V21, based on the geometry of the tailings dam as described in Fig. 1. The model used 15-noded triangular elements, ensuring a higher order of interpolation of displacements and increased accuracy. The bottom of the model was fully fixed, and the lateral boundaries were restrained against horizontal movement. The FE analysis consisted of three phases: (1) Gravity loading: This phase helped generate the initial stress field. This phase was simulated under drained condition since the rate of raising of dam raising was slow enough to not create any excess pore pressure. (2) Drainage switch: The drainage condition was switched from drained to undrained in the whole domain without applying external load. (3) Undrained loading to trigger dam failure: In this phase, small additive gravity load was applied under undrained conditions to study the stability of the drained stress state established in Phase 1. The magnitude of the additive load was chosen to be small since the dam is expected to be unstable.

4.2. NorSand Model

The NorSand model is an elastoplastic model based on the critical state theory with strain hardening (Jefferies, 1993; Jefferies and Shuttle, 2005). In the NorSand model, the initial state parameter ψ is required as an input, which is defined as the difference between the current void ratio and the corresponding critical state void ratio at the same mean effective stress (i.e., $\psi = e - e_c$). The initial state parameter ψ used in the NorSand model simulation in this work was derived from Cone Penetration Test (CPT) data (Reid, 2019). The small strain shear modulus at reference pressure level ($p_{ref} = 100kPa$) was set to be $G_{ref} = 60MPa$ for sand tailings after Morgenstern et al. (2016). The G_{ref} values for slimes were estimated based on the stiffness ratio defined in Table 1. The shear modulus was defined as a stress-dependent parameter with an exponent of$n_G = 0.45$ after Morgenstern et al. (2016). The critical stress ratio $M_{tc} = 1.33$ was derived from the effective critical state friction angle $\phi' \approx 33^{\circ}$. The CSL parameters for both sand tailings and slimes are defined in Table 2. A Poisson's ratio of $\nu = 0.3$ was assumed for all the layers. The strength parameter N and dilation limit parameter χ_{tc} (for the sand tailings in this work, $N = 0.38$, $\chi_{tc} = 7.3$) were determined from a set of drained triaxial tests on dense tailings sand. The plastic hardening parameters H_0 and H_ψ were obtained by curve fitting drained triaxial tests that included both loose and dense samples. The NorSand model parameters for both sand tailings and slimes are summarized in Table 3, and these parameters were used for the simulations in this study.

The efficiency of the NorSand model to capture the tailings behaviour was validated by comparing its predictions with laboratory test results for sand tailings, as shown in Fig. 5.

The initial void ratio for the lab test was $e_{in} = 0.8$. NorSand model required the initial state parameter ψ_0 as an input. The test that was performed under an initial confining pressure of $p_0 = 600kPa$ has a corresponding critical void ratio of $e_c = 0.71$ and thus leads to the initial state parameter $\psi_0 = 0.8 - 0.71 = 0.09$. Similarly state parameter was evaluated to be $\psi_0 = 0.07$ for $p_0 = 300kPa$, $e_c = 0.73$. The NorSand model predictions generally demonstrated good agreement with the laboratory test results, albeit with slightly smaller peak strengths and more rapid softening observed. It is important to note that the performance of NorSand can be improved by carefully adjusting the G_{ref} value. Nevertheless, $G_{ref} = 60MPa$ was maintained based on the CPT estimation.

4.3. Sanisand2004

SANISAND model is a model family that contains models built based on elastoplastic and critical state soil mechanics based model that falls under the category of bounding surface constitutive models. The concept of the state parameter was introduced into the models. The peak stress ratio and dilatancy stress ratio are related to the critical state stress ratio through the state parameter ψ. This feature allows the SANISAND model to simulate the shear behaviour of granular materials under various initial relative densities and confining pressures. SANISAND2004 is a specific version of the SANISAND model that is capable of quantitatively simulating monotonic shear behaviour and qualitatively capturing cyclic performance. The model can be calibrated based on drained/undrained triaxial test results. A detailed calibration procedure can be found in the work of Dafalias and Manzari (2004). In SANISAND2004, the power law critical state line (CSL) is used, as shown in Equation (3). The CSL parameters for SANISAND2004 for sand tailings were determined based on the information presented in Fig. 3 and were summarized in Table 2. The calibrated SANISAND2004 model parameters for both sand tailings and slimes were provided in Table 4. The detailed calibration procedure for other model parameters is not included in this paper for brevity. To evaluate the prediction efficiency of the SANISAND2004 model for sand tailings, simulation results were compared to laboratory test data, as shown in Fig. 6. However, there was no available laboratory test data to validate the SANISAND2004 model performance for slimes.

4.4. Finite element results

In the following section, the numerical simulation results will be discussed. The capabilities and limitations of each constitutive model will be discussed, and comparisons of the model performance with other constitutive models will be presented.

The state parameter ψ of the sand tailings was found to vary between 0.01 and 0.05 based on laboratory tests (Reid, 2019). Reid (2019) suggested using the 80th percentile ψ value of 0.012 derived from CPTu data for the top 20 m soil layer, where the 80th percentile ψ indicated state parameter value larger than 80 % of the statistical data. In this study, a state parameter $\psi = 0.02$ was selected for the sand tailings, which falls between the laboratory measurements and CPTu data. A

Table 2
Equation constants to determine the critical state line of different materials.

Material	Fines content	Equation (2)		Equation (3)		
		Γ	λ	e_{c0}	λ	ξ
Sand tailings and isolated slimes	40 %	0.865	0.024	0.965	0.21	0.1
Interbedded slimes	50 %	0.889	0.024	1.01	0.21	0.1
Mixed sand and slimes	70 %	1.04	0.024	1.16	0.21	0.1

Table 3
NorSand model parameters for sand tailings and slimes.

Variable	G_{ref}	p_{ref}	n_G	ν	Γ	λ_e	M_{tc}	N	χ_{tc}	H_0	H_ψ	R	ψ_0
Value	*	100	0.45	0.3	**	0.024	1.33	0.38	7.3	156	756	1	/

* : $G_{ref} = 60MPa$ is calibrated for the sand tailings. For slimes, G_{ref} is estimated based on the stiffness ratio presented in Table 1. Interbedded slimes: $G_{ref} = 60 \times 0.83 = 49MPa$; Mixed sand and slimes: $G_{ref} = 60 \times 0.58 = 35MPa$.
** : Γ values are summarized in Table 2. Sand tailings: $\Gamma = 0.865$, Interbedded slimes: $\Gamma = 0.889$; Mixed sand and slimes: $\Gamma = 1.04$.

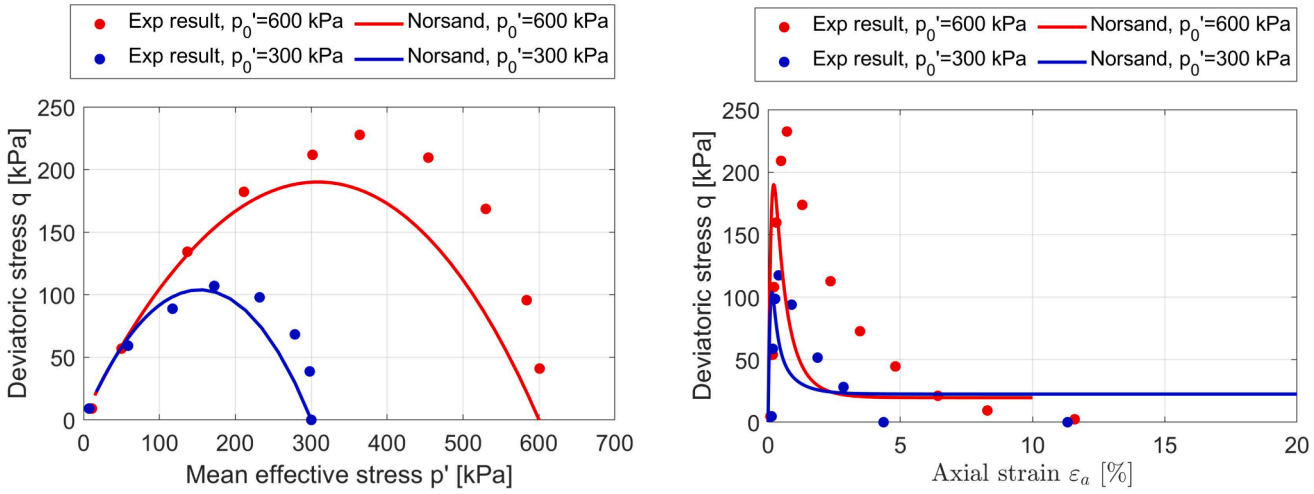

Fig. 5. NorSand model simulation results compared with undrained triaxial test results. Test conditions: $e_0 = 0.8$. The model parameters as listed in Table 3. Test data from Morgenstern et al., (2016).

Table 4
SANISAND2004 model parameters for sand tailings and slimes.

Constant	**Elasticity**		**Critical state**					**Yield**	**Plastic modulus**			**Dilatancy**		**Fabric****	
Variable	G_0	ν	M	c	λ_c	e_0	ξ	m	h_0	c_h	n^b	A_0	n^d	z_{max}	c_z
Value	*	0.05	1.31	0.725	0.21	**	0.1	0.01	4.6	0.98	1.19	0.92	2	5	600

* : $G_0 = 95$ is calibrated for the sand tailings. For slimes, G_0 is estimated based on the stiffness ratio presented in Table 1. Interbedded slimes: $G_0 = 95 \times 0.83 = 79$; Mixed sand and slimes: $G_0 = 95 \times 0.58 = 55$.
** : Sand tailings: $e_0 = 0.965$, interbedded slimes: $e_0 = 1.01$; Mixed sand and slimes: $e_0 = 1.16$ (see also Table 2).
*** : Fabric tensor parameters will not affect the current study results. Values included for completeness.

weak zone (Fig. 1) with a state parameter of $\psi = 0.09$ was detected (Reid, 2019).

The predominantly slime layer was composed entirely of fines, so it would be inappropriate to simulate this layer with the material properties of the sand tailings. Instead, it was modelled using the HS model. The HS model is a built-in model in PLAXIS, developed by Schanz et al. (1999). The HS model includes features such as an oedometer modulus dependent on effective stress, non-linear shear stress–strain behavior controlled by the mobilized angle up to the peak friction angle, and dilatancy controlled by the mobilized friction angle. Oedometer test on slime was given in panel report, without distinguishing different slime types (see Fig. 7a). Thus, in HS model calibration, all slimes were assumed to have the same oedometer modulus E_{oed}^{ref}.

The calibration of E_{oed}^{ref} was achieved by finding the best match between the simulated slime compressibility and the test results (see Fig. 7a). $E_{oed}^{ref} = 3000kPa$ along with stress-dependent component and $m = 1$, gave good agreement between HS model calculated oedometer modulus E_{oed} and those calculated from laboratory test results (Fig. 7 (b)). The unloading–reloading parameters are set to the default values of $\nu_{ur} = 0.2$ and $E_{ur}^{ref} \approx 3 \times E_{oed}^{ref} = 9000$ kPa for the slime. The coefficient of earth pressure at rest K_0^{NC} was considered as the same for slimes and sand tailings. The determination of K_0^{NC} was achieved by correlating to the sand tailings' effective friction angle as described later in the Section 6.4. The determination of the secant stiffness E_{50}^{ref} see the description in Table 5. The rest of the model parameters are determined as the same as the parameters to the sand tailings (see Section 6.4 for details). The HS model parameters for slimes are listed in Table 5.

4.5. NorSand simulation results

Reference points were defined along the failure surface (see Fig. 8) to investigate local soil behaviour during dam failure process. Among all points, only point *A* is located above the phreatic line. The failure surface initiates at the top left corner of the dam (Fig. 9c). It cuts across the

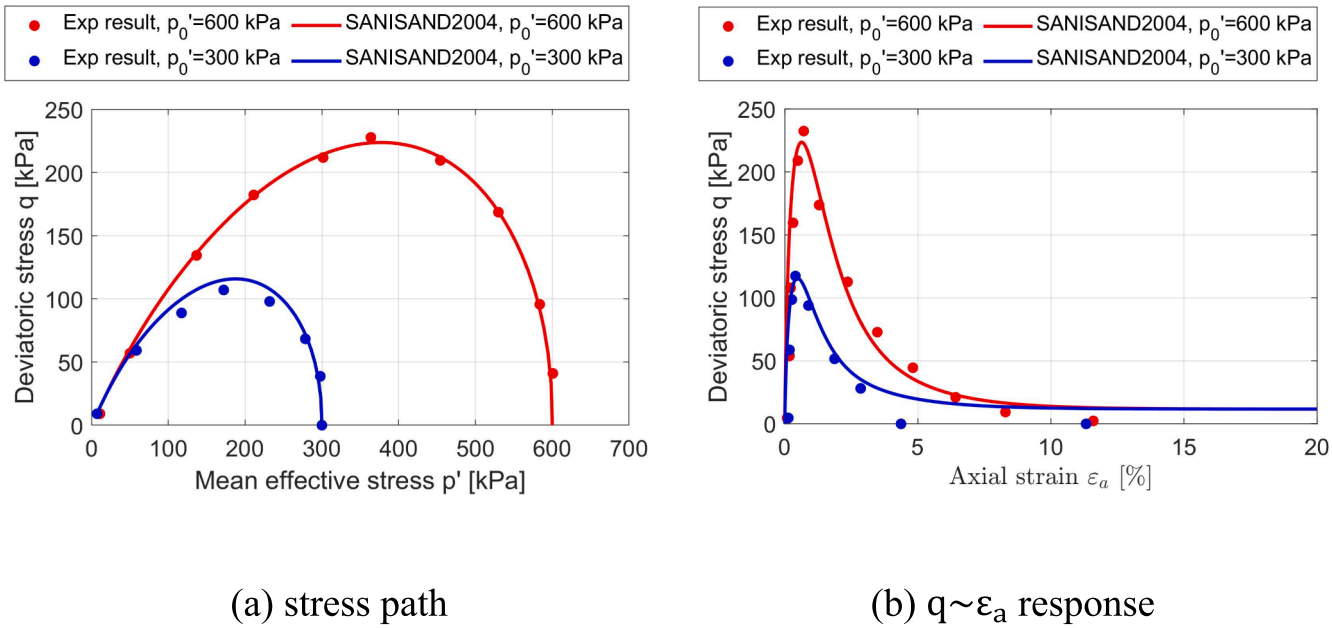

Fig. 6. SANISAND2004 model simulation results compared with undrained triaxial test results (Morgenstern et al., 2016). Test conditions: $e_0 = 0.8$. The rest model parameters see Table 4.

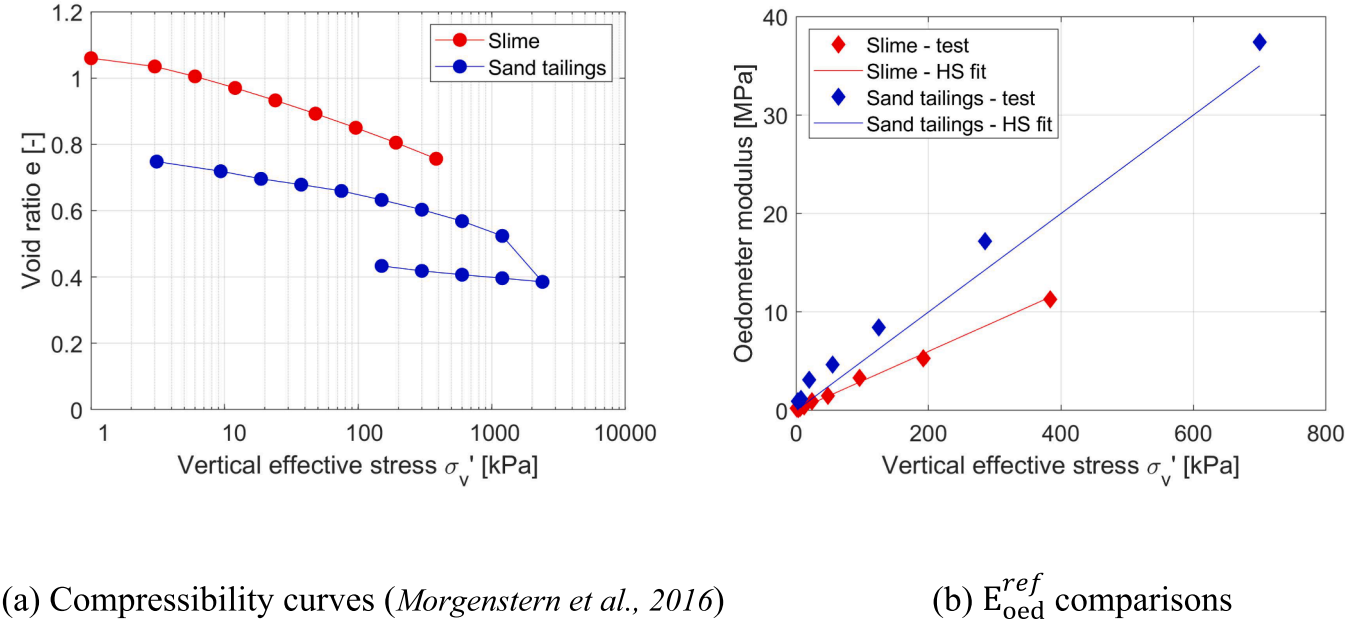

Fig. 7. Hardening soil model parameter calibration: $E_{oed}^{ref} = 5000kPa$ for sand tailings and 3000 kPa for slimes. Stress-dependent exponent m = 1 for both sand tailings and slimes.

tailings sand layer (points *A, B*), growing further into the weak layer (point *C*), and then into the interbedded slime layer (point *D*) when the additional gravity reached the peak value of 11.1%. It finally terminates by crossing the isolated slime layer in the tailings sand layer (point *E*).

Fig. 10 summarizes the local soil behaviour across the sliding surface. For point *A*, the mean effective stress p' marginally decreases with increasing deviatoric stress q (Fig. 10a) due to stress redistribution. Point *A* experiences increasing strain with increasing q (as shown in Fig. 10b) and increasing stress ratio (η, defined as $\eta = q/p'$, see Fig. 10c). Even though point *A* exists in a loose state, it is not necessarily to be saturated and is simulated as in drained loading state as it is located above the phreatic line; hence, it requires a larger perturbation to initiate instability.

For points below the phreatic line (i.e., points *B* to *E*), the mean effective stress decreases with loading (Fig. 10a). Points displayed a decrease of q soon upon loading (see Fig. 10b) and an increase of η upon loading (see Fig. 10c), except for point *E*, which was observed to experience decrease in deviatoric stress after some initial increase. The minimum residual strength was observed at point *C*, located in the weak layer, as expected. Points at shallower depths were found to experience greater soil degradation than points at deeper depths (residual strength divided by the initial deviatoric stress: point *B* < point *D* < point *E*). For points below the phreatic line (points *B* to *E*), undrained shearing led to a massive reduction in mean effective stress p', resulting in a substantial

Table 5
HS model parameters calibrated against element test results provided by Morgenstern et al. (2016).

Materials	E_{50}^{ref}[kPa]	E_{oed}^{ref}[kPa]	E_{ur}^{ref}[kPa]	m[−]	ν_{ur}[−]	K_0^{NC}[−]	p_{ref}[kPa]	c'_{ref}[kPa]	ϕ'[°]	ψ[°]	R_f[-]	POP[kPa]
Sand tailings/isolated slimes	5500	5000	15,000	1	0.2	0.455	100	1	33	−4	0.9	0
Interbedded slimes	4560*	3000**	9000	1	0.2	0.455	100	1	29.4	−4	0.9	0
Mixed sand and slimes	3190*	3000**	9000	1	0.2	0.455	100	1	23.5	−4	0.9	0
Predominated slimes	***	3000**	9000	1	0.2	0.455	100	1	***	−4	0.9	0

* : E_{50}^{ref}=5500 kPa for sand tailings and isolated slimes is determined to be similar to the E_{oed}^{ref} as explained in the main content. For Interbedded slimes and mixed sand and slimes, the value is defined as 5500 × corresponding stiffness ratios in Table 1.

** : Oedometer test on slime is given in panel report, without distinguishing different slime types. Thus, in HS model calibration, all slimes are assumed to have the same oedometer modulus.

*** : The value is difficult to determined due to the big difference on the stiffness properties among predominantly slimes and other materials (as shown in Table 1). In the simulation, E_{50}^{ref}=1100 kPa and $\phi' = 20^{\circ}$ are used (lower stiffness compared to mixed sand and tailings).

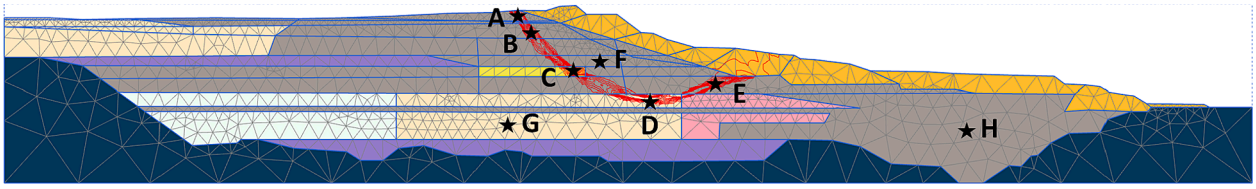

Fig. 8. Selected representative points: NorSand simulations.

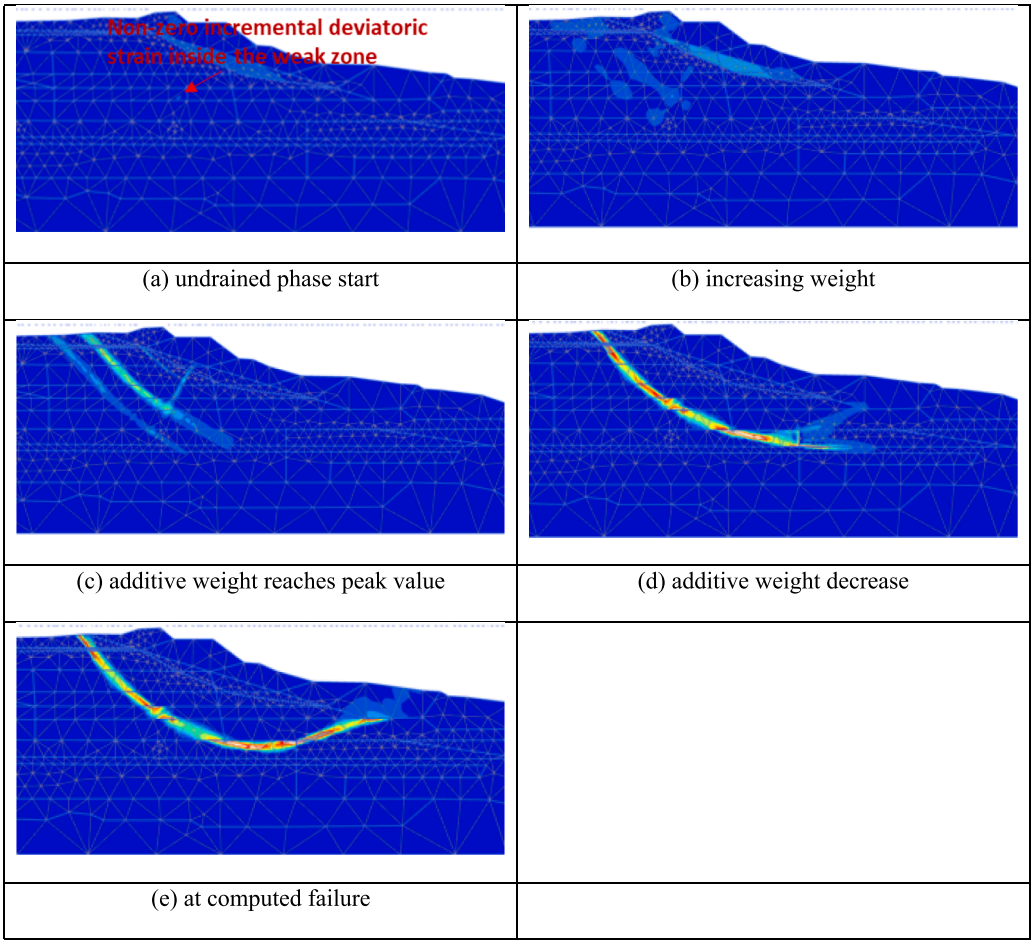

Fig. 9. Evolution of the failure surface in the undrained phase simulation: NorSand.

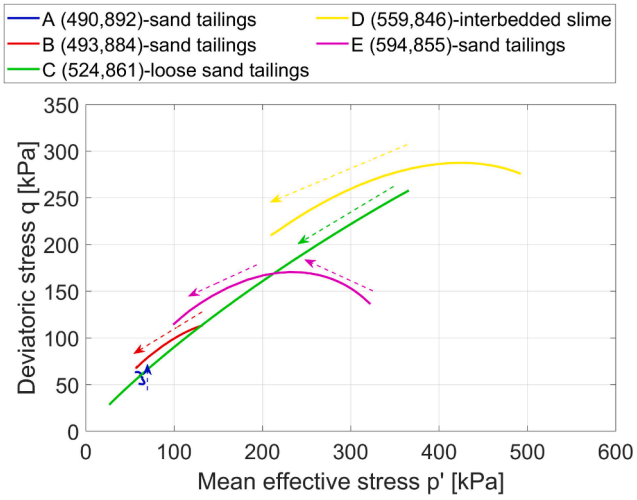

(a) stress paths

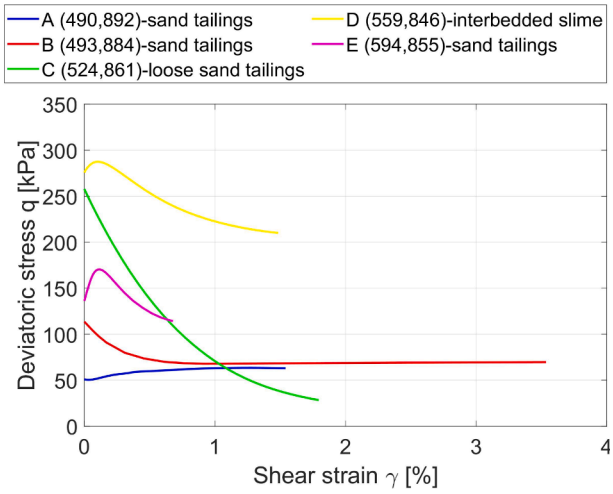

(b) stress-strain response

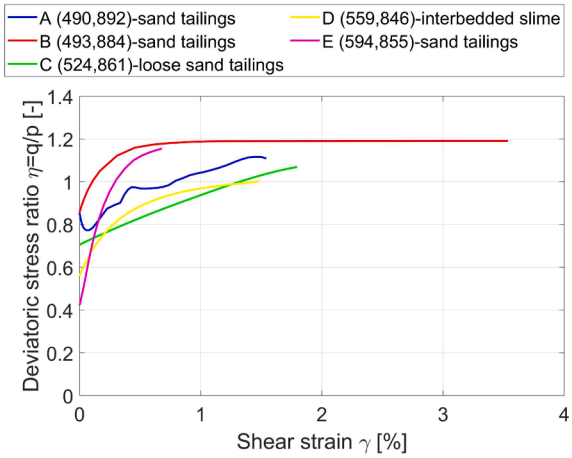

(c) stress-ratio against shear strain

Fig. 10. Local soil response simulated using NorSand. Representative points locate on the failure surface (see Fig. 8). The point labels, coordinates and material types as indicated in the plot legends. The changing patterns are indicated using dashed-line arrows.

reduction of soil stiffness. The deviatoric stress was also found to decrease with increasing external loading. The results demonstrated that following two observations under undrained conditions controlled failure:

(1) Soil layers showed a decrease in the q and p' but an increase in the stress ratio η (until instability in the soil got tiggered) when a triggering load was applied.
(2) The first factor should lead to relatively large strain, leading to the formation of failure surface.

The above two points can be investigated by applying the additional weight under drained condition. In the case of loose tailings sand under drained conditions, a much higher shear stress ratio is required to trigger instability compared to undrained conditions. For example, an additional weight of 100% could be applied under drained conditions without initiating any failure. This indicated that undrained condition was more critical in triggering instability and static liquefaction in the tailings dam. The incremental deviatoric strain distribution in Fig. 11a shows that there was no clear formation of a shear band under an additional weight of 100 % under drained conditions. Fig. 11b presents stress paths of the representative points (Fig. 8) under drained perturbation. To compare drained and undrained stress paths, undrained stress paths are marked with dashed lines in Fig. 11b. Under the drained situation, points A, B, D, and E experienced an increase in both effective mean stress p' and deviatoric stress q. Unlike the undrained case, the shear stress ratio of these points experienced a decrease under the drained condition.

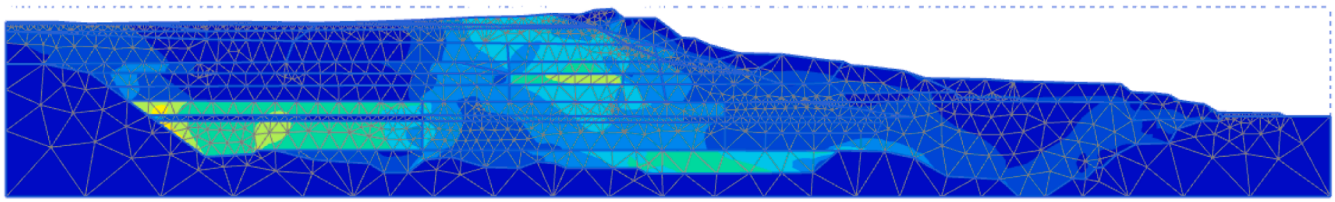

(a) incremental deviatoric strain distribution

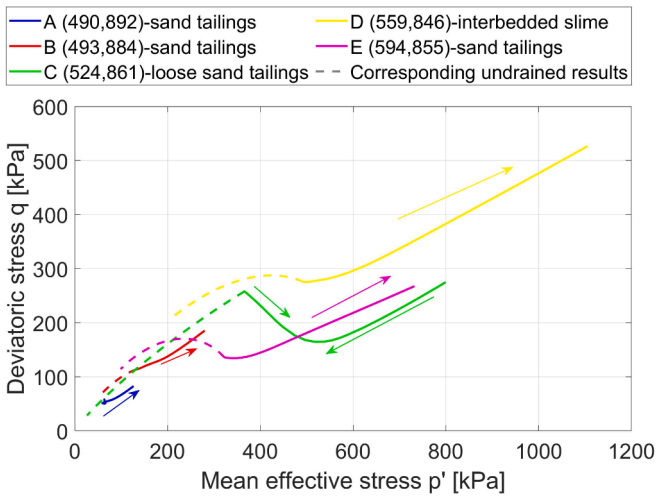

(b) stress path of the selected points

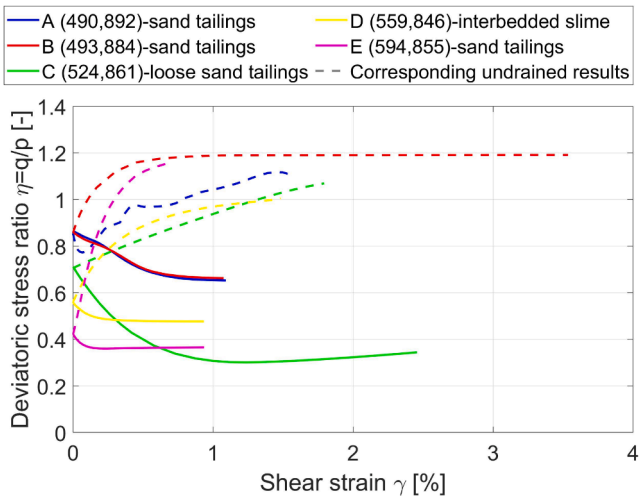

(c) stress ratio against shear strain

Fig. 11. Local soil response under fully drained weight increase (with additive weight up to 1-time the self-weight). Representative points locate on the failure surface: points A-E lie inside the failure surface, points F-H are outside, as shown in Fig. 8. In the plots, solid lines represent for 'Drained case' and dashed-lines represent for 'Undrained'.

4.6. Sanisand2004

To achieve a uniform distribution of the initial state parameter (in this case, 0.02) in the SANISAND2004 model, the value of the initial void ratio required indirect estimation. This was accomplished by determining the state parameter from the local mean effective stress and void ratio based on the pre-determined CSL. After applying gravity, the local effective confining pressure within the dam varies with depth. To obtain a uniform distribution of state parameter throughout the entire dam, the dam should be discretized into multiple layers. The void ratio of each layer was calculated through a trial-and-error process to achieve $\psi = 0.02$ at the centre of the layer. In this work, the entire dam was divided into three parts, with an initial void ratio e_{in} as described in Fig. 12. The predominated slimes layer was simulated using the HS model with material parameters as tabulated in Table 5 in Section 6.

The evolution of the sliding surface (incremental deviatoric strain) was illustrated in Fig. 13. It includes zone with significant incremental deviatoric strains (the zone illustrated by the dashed-line box in Fig. 1). Incremental deviatoric strain was observed both along the top east crest of the dam above the phreatic line and at the bottom of the dam (as shown in Fig. 13a, within the mixed sand and slime layer). As additional weight was applied, distinct incremental deviatoric strain extended towards the crest of the dam (Fig. 13b), eventually forming a clear sliding surface. Around peak additional weight of 7%, the sliding surface expanded further, as evident in Fig. 13c. Further as the additional weight kept decreasing, incremental deviatoric strains continued to

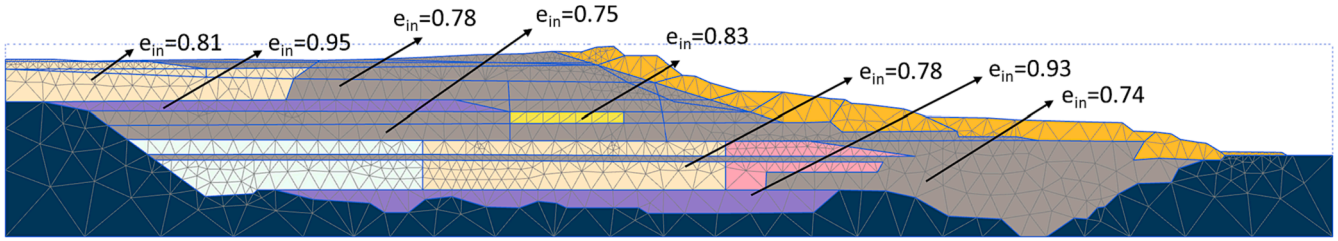

Fig. 12. Initial void ratio distribution in the tailings dam when using SANISAND2004.

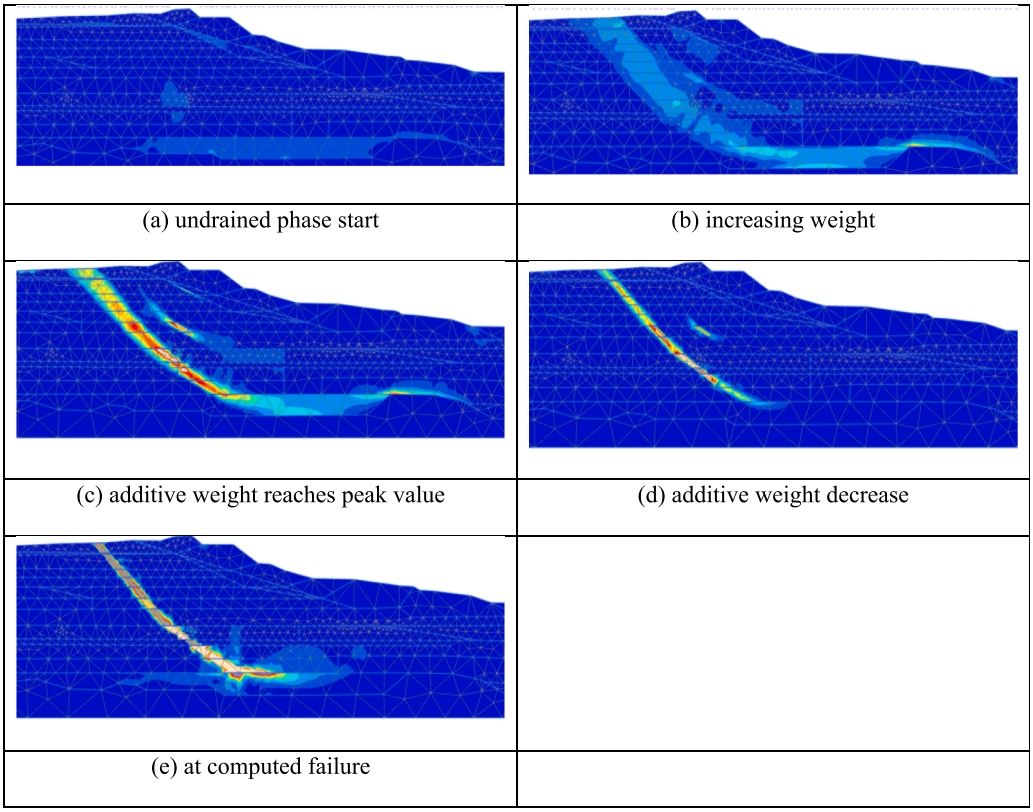

Fig. 13. Evolution of the failure surface in the undrained phase simulation: SANISAND2004.

grow in the shallow layers of the dam compared to deeper layers near the toe (Fig. 13d). At point of failure, a clear sliding surface was formed (Fig. 13e), with large incremental deviatoric strain in deeper layers (mixed sand and slime layer). This indicates that the mixed sand and slime layer predominantly contributes to dam failure. One plausible reason for this could be targeting to achieve a state parameter value of 0.02 at the centre of each layer. This might have led to deeper layer experiencing higher mean effective stresses at points below the midpoint of the layer, leading to higher positive values of state parameter. Higher positive state parameter values make the layer more prone to collapse under undrained conditions, resulting in higher levels of pore water pressure under the similar level of shear. This eventually contributes to the failure of the dam.

Eight reference points are defined to study the local material behavior during the dam failure process, as illustrated in Fig. 14).

Point *A'* is located above the phreatic line. The failure surface initiates at the top of the dam and cuts across layers of sand tailings (where points *A'* and *B'* are located), further below, points *C'* and *F'* are within the loose sand tailings layer, points *E'* and *G'* are within the interbedded slimes layer, and finally, the failure surface terminates in the mixed sand and slime layer, where Point *H'* is located.

The soil responses in the form of shear stress–strain, mean effective stress, and deviatoric stress plots of reference points are shown in Fig. 15.

he points below the phreatic line (i.e., points *B'* to *G'*) experience a decrease in shear stress as soon as they are loaded and undergo continuous loss of mean effective stress with increasing deviatoric stress (as shown in Fig. 15a). These points below the phreatic line lose nearly 40 % of their material strength upon undrained loading, indicating a potentially unstable effective stress state of the soil upon gravity loading. Subsequently, any change from drained condition to undrained condition coupled with a small, rapid perturbation will lead to a drastic reduction in shear stress, resulting in a progressive kind of failure. However, points located outside the sliding surface (point *H'*) experience no significant changes with respect to the mean effective stress and deviatoric stress (as illustrated in Fig. 15a). Fig. 15c depicts that all sand tailings points experience an increase in the stress ratio with increasing shear strain – which is identical with the observations from the NorSand simulation results. Fig. 13 and Fig. 15 together indicate that the formation of the sliding surface is closely linked to an increase in stress ratio under the condition of reducing deviatoric stress and decreasing mean effective stress.

It has been demonstrated that abrupt dam failure requires a small perturbation under undrained condition. In this work, the minimum perturbation was found to be 7.4 %. Magnitude of perturbation required depends on the effective stress state which eventually depends on the construction sequence of the dam. This concludes that improper construction or design might lead to static liquefaction.

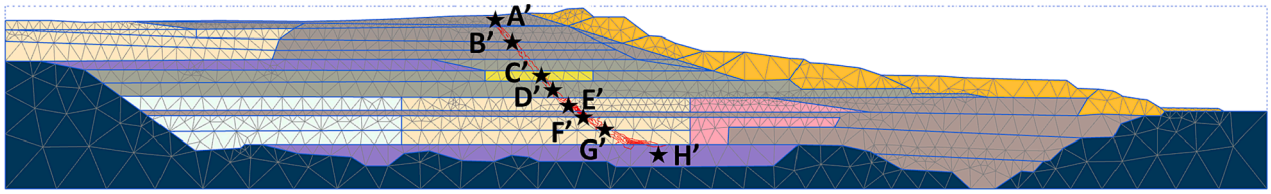

Fig. 14. Selected representative points: SANISAND2004 simulations.

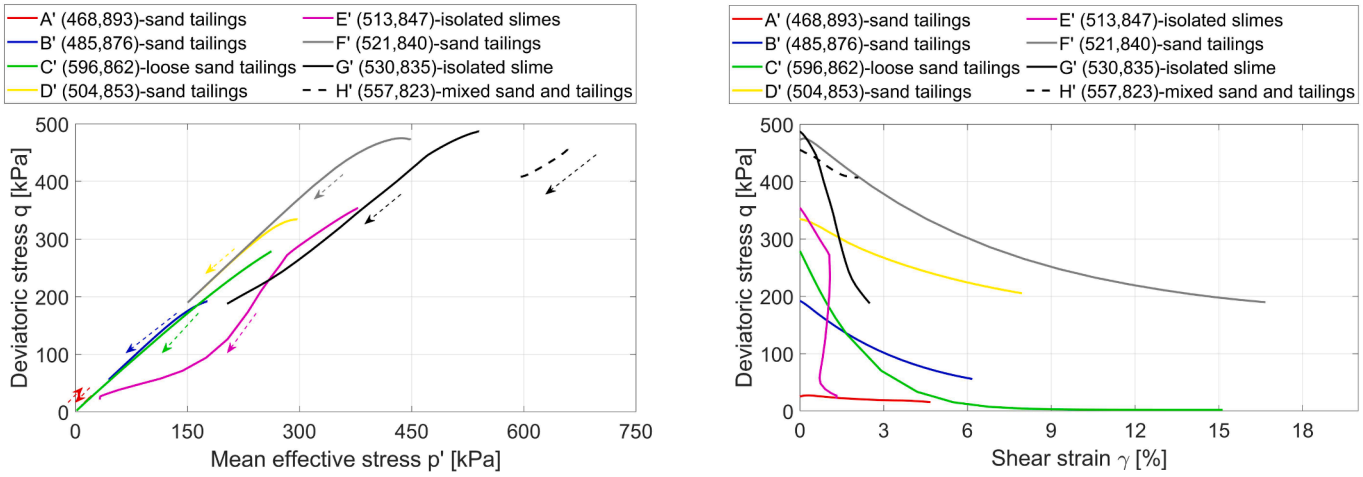

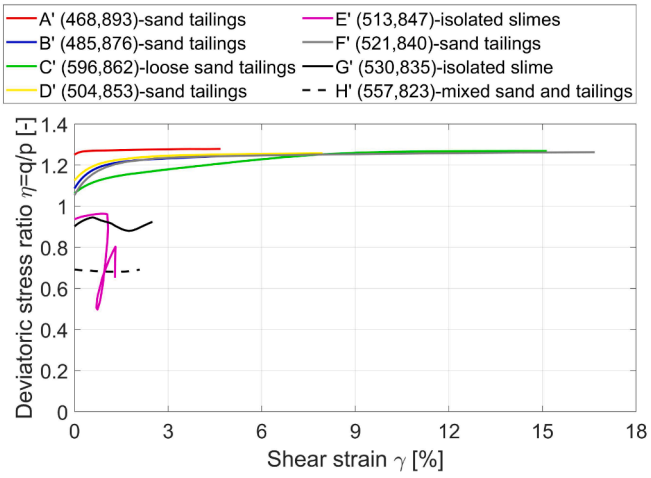

Fig. 15. Local soil response simulated using SANISAND2004. Representative points located on the failure surface (see Fig. 14). The point labels, coordinates and material types as indicated in the plot legends. The changing patterns are indicated using dashed-line arrows.

To validate the aforementioned conclusion, confirmatory simulations were conducted by applying additional portion of self-weight of the tailing dam, starting from different heights (initial heights of 92*m* and 100*m* were considered). The correlation between the additional self-weight required to induce failure and the dam construction height is illustrated in Fig. 16. For a dam with a height of 81*m*, 15.9% additional self-weight is needed to trigger dam failure. However, this requirement decreases to 7.4% for a dam height of 92*m* and further reduces to 4.7% for a dam height of 100*m*.

5. Discussion

5.1. Soil state parameter effect

To simulate static liquefaction mode of failure, a framework based on the state parameter ψ was established. Two advanced constitutive models, SANISAND2004 and NorSand, were selected due to their capabilities to capture diffuse failure. In this work, the simulations considered a uniform material state parameter of $\psi = 0.02$ for entire tailings dam, except for the weak zone, where state parameter of $\psi = 0.09$ was considered. This assumption was made on the basis of available CPTu test data and laboratory test results. However, it should be noted that the CPTu data only included information for the first 20 m of soil depth, while the entire height of the dam was about 92 m. The lack of ψ information (or more generally, the missing CPTu data) for the remaining depth can significantly impact the performance of the simulation, especially because the reduction of the mean effective stress under undrained conditions is closely linked to the magnitude of ψ. Another source of uncertainty regarding the state parameter is its variability across the entire geometry. It is impractical for the entire material in the dam to undergo static liquefaction simultaneously. Instead, static liquefaction tends to manifest in localized unstable zones within the

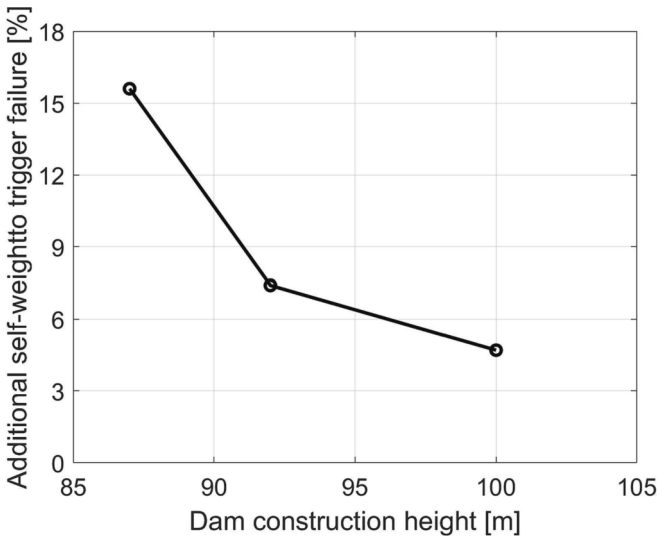

Fig. 16. Relationship between the dam construction height and the required additional self-weight to trigger failure.

tailings dam. This localized initiation then propagates from these zones, eventually resulting in a global dam collapse. Consequently, when compared to the scenario of a uniformly distributed state parameter, the spatial variability of the state parameter may lead to a shift in the initial unstable zone, potentially altering the position of the sliding surface and the magnitude of the perturbation load.

5.2. Weak-layer effect

A weak layer was detected by the CPTu, as reported by Reid (2019). The role of the weak layer was studied by replacing the weak layer material in Fig. 1 with the adjacent material. The required additional self-weight for the NorSand simulation to trigger dam failure increased from 11.1% to 12.5% if the weak layer was ignored. For the SANISAND2004 simulation, it increased from 7.4% to 9.0%. Results indicated that presence of weak layer marginally increases the possibility of dam failure. However, the NorSand simulation results suggest that careful detection of the weak layer is necessary, as the propagation of the sliding surface might start from the weak layer. This indicates that the weak layer could play a crucial role in the initiation of dam failure, and its proper identification is important for assessing the stability of the tailings dam accurately.

5.3. Fines content effects

The tailings dam studied in this work contains zones with slime material. The fines content in the slimes certainly affects the local material behaviour and, consequently, the overall dam stability. The approach adopted in this work is to account for the effects of fines content by varying the positions of material critical state lines (CSL) while keeping the same CSL shape, as indicated by Yin et al. (2016). The changes in material critical state stress ratio and stiffness due to the variation in fines content are considered based on the material test report (Morgenstern et al., 2016). When performing FE simulations using CSL-based advanced constitutive models, the other parameters were kept similar to that of pure sand model parameters. This was done for simplicity assuming that fines content had no effect on the other model parameters. However, the model parameters linked to stiffness often exhibit interdependence with those related to the critical state line. Changes in fines content within the soil prompt adjustments in critical state line-related model parameters, subsequently influencing other aspects of the model. Calibration of these parameters becomes imperative and should be carried out through tests conducted on the corresponding soil. To achieve this, two key activities must be undertaken: (1) conducting reliable laboratory tests to establish material-specific relationships between fines content and CSL, and (2) adjusting the constitutive model for each material (or fines content level) based on the outcomes of the laboratory tests.

5.4. Initial stress field and selection of constitutive model

Both the NorSand and SANISAND2004 models can effectively capture static liquefaction behavior. As mentioned, the soil's instability is closely related to the stress state before the application of perturbation. The stress state prior to the dam failure was investigated to investigate the stress states of the selected representative points that were on the potential failure surface in NorSand and SANISAND2004 simulations. The hardening soil model (HS) simulation was used as benchmark owing to its accurate simulation of soil compressibility, as demonstrated in Fig. 7.

The model parameters are listed in Table 5. The calibration of HS model parameters for the slimes has been discussed in Section 5. In this section, the calibration of HS model parameters for sand tailings are discussed. The sand tailings have friction angle of $\phi^{'} = 33^{\circ}$, as suggested by Morgenstern et al. (2016). $K_0^{NC} = 1 - sin\phi^{'} = 0.455$ was considered. The oedometer modulus E_{oed} was determined from compressibility curves as presented in Fig. 7(a). The tangent stiffness at the reference vertical stress E_{oed}^{ref}, was picked to be 5000 kPa. Due to lack of sufficient drained triaxial test data, secant stiffness E_{50}^{ref} was taken to be approximately the same as E_{oed}^{ref} (in this work, $E_{50}^{ref} = 5500kPa$ for sand tailings). The unloading–reloading Poisson's ratio $\nu_{ur} = 0.2$ and Young's modulus $E_{ur}^{ref} \approx 3 \times E_{oed}^{ref} = 15000$ kPa. A small coefficient value $c_{ref}^{'} = 1\,kPa$ was selected. The failure ratio R_f is assumed to be 0.9. The rest of the model parameters are determined using a trial-and-error approach to achieve the best match between the drained triaxial test results ($e_{in} = 0.71, p_{in} = 300kPa$) and HS model predictions. A dilatancy angle of -4° was chosen to ensure that the volumetric strain coincides with the laboratory measurements at large axial strain, as shown in Fig. 17.

In this work, the HS model simulation follows a staged construction procedure for the tailings dam. The evaluation of the stress state prior to the undrained perturbation in NorSand and SANISAND2004 simulations can be compared with the HS simulated stress state, as shown in Fig. 18.

From Fig. 18, it can be observed that the NorSand model gave larger effective mean stress (p') prior to undrained loading compared to the HS simulation results. The stress ratio obtained using the NorSand model is lower than that obtained using the HS model. On the other hand, the SANISAND2004 model generally gave smaller mean effective stress (p'), larger deviatoric stress (q), and slightly larger stress ratio (η). The larger stress ratio in the SANISAND2004 model may explain why it requires a smaller perturbation to trigger dam instability compared to the NorSand model. It concludes that uncertainties in the calculated stress states may affect the calculation of the corresponding undrained stability.

5.5. Model platform and parameter selection

Most of the NorSand model parameters can be directly obtained from laboratory test data or correlations based on CPT data. On the other hand, SANISAND2004 model requires calibration of additional model parameters–but can also be easily modified to incorporate extra features such as anisotropic critical state theory to better simulate principal stress rotation as proposed by Petalas et al. (2019), or simulate sand cyclic ratcheting behaviour as shown by Liu et al., (2019, 2020; Liu and Kaynia (2023). Both models require sufficient test data (laboratory element and CPTu correlations) to achieve high-quality material parameters for reliable simulation results.

In this study, upon comparing the calibration outcomes of the two models (i.e., from the Norsand model calibration results in Fig. 5 to the

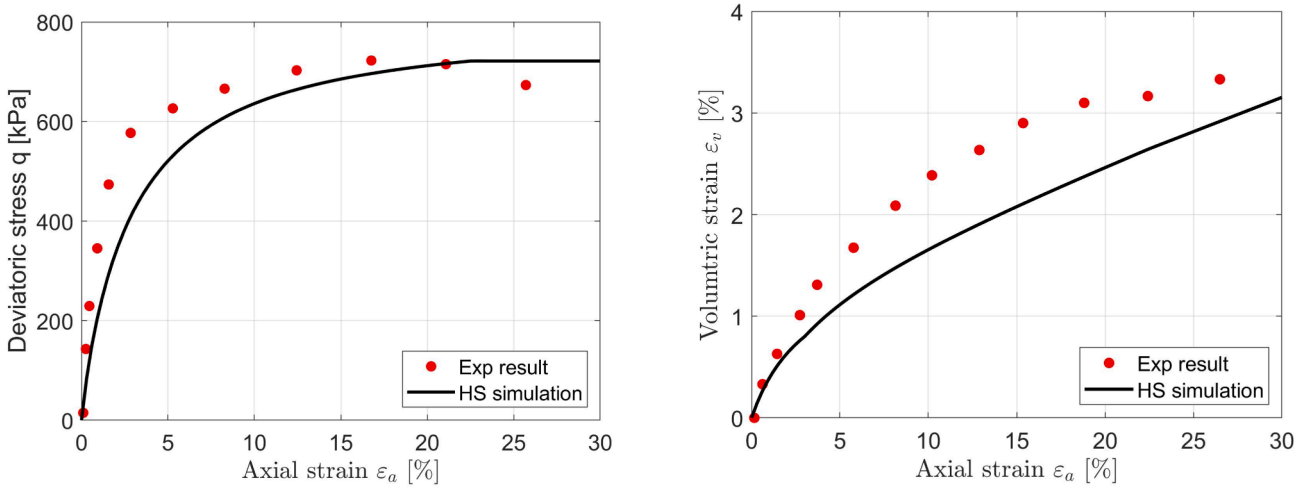

(a) $q \sim \varepsilon_a$ response (b) $\varepsilon_v \sim \varepsilon_a$ response

Fig. 17. Hardening soil model simulation results compared with drained triaxial test results. Test conditions: $e_0 = 0.71$, $p'_{in} = 300kPa$. Test data from Morgenstern et al., (2016).

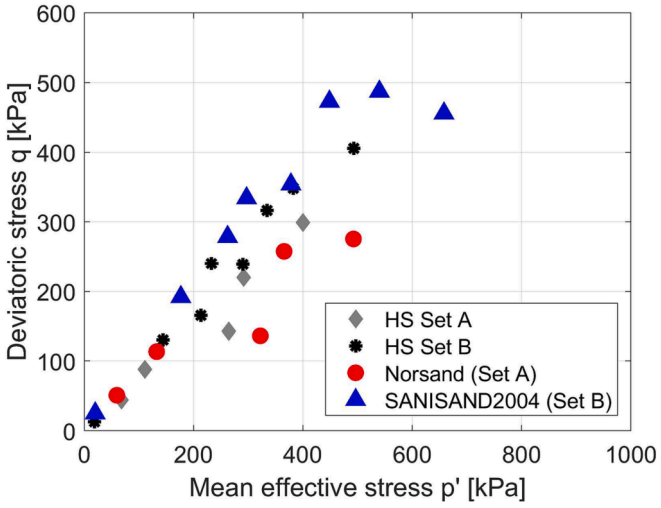

Fig. 18. Initial effective stress conditions of the selected points. The points Set A correspond to points A-E in Fig. 8; the points Set B correspond to points A'-H' in Fig. 14.

SANISAND2004 model calibration results in Fig. 6), it becomes apparent that the Norsand model predicts a smaller undrained strength using the model parameters summarized in Table 3. Consequently, under otherwise identical soil, loading, and simulation conditions, it is anticipated that the simulation using the Norsand model would require less additional load compared to the SANISAND2004 to induce static liquefaction. However, in this investigation, due to non-identical initial state parameters and initial stress ratios (refer to Fig. 18) generated in the tailings dam domain, the simulation using the SANISAND2004 model required less external load to trigger static liquefaction.

6. Concluding remarks

It was demonstrated that critical state soil mechanics based constitutive model was a necessity to capture diffuse kind of failure in tailings material leading to static liquefaction and progressive failure of a tailings dam in Brazil. Both the NorSand model and SANISAND2004 were shown to be capable of capturing reduction in shear stress with increasing shear strain at critical drained stress states. The stability of the tailings dam was perturbed by a small increase in gravity load under undrained conditions, such a simulation method is believed to be a good representation of static liquefaction triggering mechanism. The progressive development of the failure mode was simulated using the arc-length method available in PLAXIS. Reliable estimation of state parameter across dam height was highlighted. Input to quantify the variation of state parameter depends on the choice of constitutive model and hence, choice should be made in accordance to the data available from field and laboratory data. Methodology is developed to account for effect of fines in slimes by changing the critical state line and the soil strength based on published results on other sands with fines. The presented procedure is believed to be beneficial for investigating tailings dam stability and can be an efficient tool to support risk management decisions.

CRediT authorship contribution statement

Haoyuan Liu: . **Sparsha Nagula:** . **Hans Petter Jostad:** . **Luca Piciullo:** Funding acquisition, Investigation, Project administration, Writing – original draft. **Farrokh Nadim:** Conceptualization, Methodology, Supervision.

Declaration of Competing Interest

The authors declare that they have no known competing financial interests or personal relationships that could have appeared to influence the work reported in this paper.

Data availability

Data will be made available on request.

Acknowledgements

The research activities carried out are finically supported by the Norwegian Geotechnical Institute research project SP12 – Sustainable and safe mine tailings. The authors gratefully acknowledge the Norwegian Geotechnical Institute.

Appendix A. Supplementary data

Supplementary data to this article can be found online at https://doi.org/10.1016/j.compgeo.2024.106089.

References

Brinkgreve, R. B. J., Kumarswamy, S., Swolfs, W. M., Waterman, D., Chesaru, A., & Bonnier, P. G. (2016). PLAXIS 2016. PLAXIS bv, the Netherlands.

Brzezinski, L.S., 2002. Static Liquefaction as a Possible Explanation for the Merriespruit Tailings Dam Failure: Discussion. Canadian Geotechnical Journal 39 (6), 1439–1440.

Chakrabotry, D., Choudhury, D., 2009. Investigation of the Behavior of Tailings Earthen Dam under Seismic Conditions. American Journal of Engineering and Applied Sciences 2, 559–564.

Dafalias, Y.F., Manzari, M.T., 2004. Simple plasticity sand model accounting for fabric change effects. Journal of Engineering mechanics 130 (6), 622–634.

Gens, A., 2019. Hydraulic fills with special focus on liquefaction. In Proceedings of the XVII ECSMGE-2019: Geotechnical Engineering foundation of the future. In: International Society for Soil Mechanics and Geotechnical Engineering (ISSMGE), pp. 1–31.

Glotov, V.E., Chlachula, J., Glotova, L.P., Little, E., 2018. Little Causes and environmental impact of the gold-tailings dam failure at Karamken, the Russian Far East. Engineering Geology 245, 236–247.

Guo, Z., Chen, L., Yin, K., Shrestha, D.P., Zhang, L., 2020. Quantitative Risk Assessment of Slow-Moving Landslides from the Viewpoint of Decision-Making: A Case Study of the Three Gorges Reservoir in China. Engineering Geology 273, 105667.

Jefferies, M.G., 1993. Nor-Sand: a simle critical state model for sand. Géotechnique 43 (1), 91–103.

Jefferies, M. G., & Shuttle, D. A. (2005). NorSand: features, calibration and use. In Soil constitutive models: evaluation, selection, and calibration (pp. 204-236).

Jefferies, M., Been, K., 2006. Soil liquefaction: A critical state approach. Taylor & Francis, CRC Press, London, London.

Li, X.S., Dafalias, Y.F., 2000. Dilatancy for cohesionless soils. Dilatancy for cohesionless soils. Géotechnique 50 (4), 449–460.

Liu, H.Y., Abell, J.A., Diambra, A., Pisanò, F., 2019. Modelling the cyclic ratcheting of sands through memory-enhanced bounding surface plasticity. Géotechnique 69 (9), 783–800.

Liu, H.Y., Diambra, A., Abell, J.A., Pisanò, F., 2020. Memory-enhanced plasticity modeling of sand behavior under undrained cyclic loading. Journal of Geotechnical and Geoenvironmental Engineering 146 (11), 04020122.

Liu, H., Kaynia, A.M., 2023. Characteristics of cyclic undrained model SANISAND-MSu and their effects on response of monopiles for offshore wind structures. Géotechnique 73 (4), 294–309.

Martin, T.E., McRoberts, E.C., 1999. (January). Some considerations in the stability analysis of upstream tailings dams, 99. AA Balkema, Rotterdam, Netherlands, pp. 287–302.

Morgenstern, N.R., Vick, S.G., Viotti, C.B., Watts, B.D., 2016. Fundão tailings dam review panel: Report in the immediate causes of the failure of the Fundão Dam. Cleary Gottlieb Steen & Hamilton LLP, New York.

Nicot, F., Daouadji, A., Laouafa, F., Darve, F., 2011. Second-order work, kinetic energy and diffuse failure in granular materials. Granular Matter 13 (1), 19–28.

Petalas, A.L., Dafalias, Y.F., Papadimitriou, A.G., 2019. SANISAND-FN: An evolving fabric-based sand model accounting for stress principal axes rotation. International Journal for Numerical and Analytical Methods in Geomechanics 43 (1), 97–12 3.

M.B. Peter S.K. Mahmood Seismic Stability of Impoundments 2003 Vancouver, British Columbia 77 84.

Piciullo, L., Storrøsten, E.B., Liu, Z., Nadim, F., Lacasse, S., 2022. A new look at the statistics of tailings dam failures. Engineering Geology 303, 106657.

Reid, D., 2019. Additional analyses of the Fundao tailings storage facility: in situ state and triggering conditions. Journal of Geotechnical and Geoenvironmental Engineering 145 (11), 04019088.

Roscoe, K.H., Schofield, A.N., Wroth, C.P., 1958. On The Yielding of Soils. On the yielding of soils. Géotechnique 8 (1), 22–53.

Rotta, L.H.S., Alcantara, E., Park, E., Negri, R.G., Lin, Y.N., Bernardo, N., Mendes, T.S.G., Sousa Filho, C.R., 2020. The 2019 Brumadinho tailings dam collapse: possible cause and impacts of the worst human and environmental disaster in Brazil. International Journal of Applied Earth Observation and Geoinformation. 90 (10), 1016.

Sadrekarimi, A., 2014. Static liquefaction-triggering analysis considering soil dilatancy. Soils and foundations 54 (5), 955–966.

Sadrekarimi, A., 2016. Static liquefaction analysis considering principal stress directions and anisotropy. Geotech Geol Eng 34 (4), 1135–1154. https://doi.org/10.1007/s10706-016-0033-7.

Schanz, T., Vermeer, P.A., Bonnier, P.G., 1999. In: The hardening soil model: formulation and verification. Balkema, Rotterdam, the Netherlands, pp. 281–296.

Schofield, A.N., Wroth, C.P., 1968. Critical state soil mechanics. McGraw-Hill Book Co., London.

Tang, Y., Guo, Z., Wu, L.i., Hong, B.o., Feng, W., Su, X., Li, Z., Zhu, Y., 2022. Assessing Debris Flow Risk at a Catchment Scale for an Economic Decision Based on the LiDAR DEM and Numerical Simulation. Frontiers in Earth Science 10, 821735.

Terzaghi, K., 1957. Varieties of submarine slope failure. Norwegian Geotechnical Institute, Publication 25, 1–16.

Wang, T., Zhou, Y., Lv, Q., Zhu, Y., Jiang, C., 2011. A Safety Assessment of the New Xiangyun Phosphogypsum Tailings Pond. Minerals Engineering 24 (10), 1084–1090.

Wei, Z., Yin, G., Wang, J.G., Wan, L., Li, G., 2013. Design, construction and management of tailings storage facilities for surface disposal in China: case studies of failures. Waste Management and Research 31 (11), 106–112.

Yin, Z.Y., Huang, H.W., Hicher, P.Y., 2016. Elastoplastic modeling of sand–silt mixtures. Soils and foundations 56 (3), 520–532.

Yu, D., Tang, L., Chen, C., 2020. Three-dimensional numerical simulation of mud flow from a tailing dam failure across complex terrain. Natural Hazards and Earth System Sciences 20, 727–741.

Zandarín, M.T., Oldecop, L.A., Rodríguez, R., Zabala, F., 2009. The Role of Capillary Water in the Stability of Tailing Dams. Engineering Geology 105 (1-2), 108–118.